

Least but not Last: Fine-tuning Intermediate Principal Components for Better Performance-Forgetting Trade-Offs

Alessio Quercia^{1,2} Arya Bangun¹ Ira Assent^{1,3} Hanno Scharr¹

Abstract

Low-Rank Adaptation (LoRA) methods have emerged as crucial techniques for adapting large pre-trained models to downstream tasks under computational and memory constraints. However, they face a fundamental challenge in balancing task-specific performance gains against catastrophic forgetting of pre-trained knowledge, where existing methods provide inconsistent recommendations. This paper presents a comprehensive analysis of the performance-forgetting trade-offs inherent in low-rank adaptation using principal components as initialization. Our investigation reveals that fine-tuning intermediate components leads to better balance and show more robustness to high learning rates than first (PiSSA) and last (MiLoRA) components in existing work. Building on these findings, we provide a practical approach for initialization of LoRA that offers superior trade-offs. We demonstrate in a thorough empirical study on a variety of computer vision and NLP tasks that our approach improves accuracy and reduces forgetting, also in continual learning scenarios.

1. Introduction

The explosive growth of large-scale pre-trained models has revolutionized artificial intelligence across multiple domains, from Natural Language Processing to Computer Vision. Foundation models, often containing billions or even trillions of parameters, demonstrate remarkable capabilities in learning and in generating human-like content (Brown et al., 2020; Kaplan et al., 2020). However, their deployment in real-world applications faces significant computational and memory constraints that present considerable

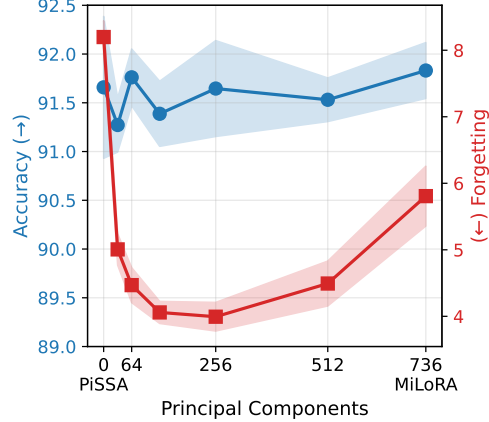


Figure 1. Accuracy (left) and forgetting (right) when fine-tuning principal components on ImageNet1k pre-trained ViT-B to Caltech101. Forgetting shows a U-shape with most information lost at the extremes where existing methods PiSSA use the main, and MiLoRA the least components, respectively.

challenges, in particular in continual learning scenarios, which require constant knowledge updates.

Traditional fine-tuning approaches require updating of all model parameters, leading to substantial computational and memory requirements, which can be prohibitive for many applications (Houlsby et al., 2019; Stickland & Murray, 2021). For instance, fine-tuning a large language model with billions of parameters demands enormous GPU memory and computational resources, making it inaccessible to institutions with limited compute resources or financial budget. This bottleneck is compounded when models need to be adapted to multiple downstream tasks or domains, as each adaptation traditionally necessitates a complete copy of the fine-tuned model.

Parameter-Efficient Fine-Tuning (PEFT) methods have emerged as a promising solution, enabling effective adaptation of large models with significantly reduced resource requirements (Hu et al., 2021; Liu et al., 2024; Kopiczko et al., 2023; Quercia et al., 2025a; Meng et al., 2024; Wang et al., 2024a; Zaken et al., 2021; Xie et al., 2023). Among the most notable approaches, Low-Rank Adaptation (LoRA) (Hu et al., 2021) constrains weight updates to low-rank ma-

¹IAS-8, Forschungszentrum Juelich, Juelich, Germany

²Department of Computer Science, RWTH Aachen University, Aachen, Germany ³Aarhus University, Aarhus, Denmark. Correspondence to: Alessio Quercia <a.quercia@fz-juelich.de>.

trices, which has been shown to preserve much of the pre-trained knowledge while requiring only a small fraction of the parameters for tuning. Notably, as (Biderman et al., 2024) states “*LoRA learns less and forgets less*”, indicating LoRA’s advantage in retaining pre-trained capabilities, especially important in continual learning applications.

LoRA has attracted substantial attention in the research community and inspired numerous extensions, including DoRA (Liu et al., 2024), which decomposes weights into magnitude and direction components, while VeRA, (Kopczko et al., 2023), introduces a vector-based random matrix adaptation for further parameter reduction. More recent advancements include PiSSA (Meng et al., 2024) and MiLoRA (Wang et al., 2024a), which respectively initialize LoRA modules with essential principal components for better adaptation, and minor principal components to reduce forgetting. Other PEFT methods study alternative approaches like BitFit (Zaken et al., 2021), which only updates bias terms, and DiffFit (Xie et al., 2023), which specializes in diffusion model adaptation through targeted adjustments to scaling factors and biases.

Despite their efficiency, PEFT methods face a challenge that has been relatively understudied: the *performance-forgetting trade-off*. While PEFT approaches excel at task adaptation with minimal resource investment, they risk sacrificing original pre-trained knowledge (Chen et al., 2022; Dai et al., 2023). While LoRA emphasizes the importance of learning more and forgetting less (Biderman et al., 2024), the precise relationship between rank, adaptation capacity, and catastrophic forgetting remains an open question.

Recent studies introduce the idea of using principal components to initialize LoRA modules (Meng et al., 2024; Wang et al., 2024a), where MiLoRA explicitly targets the performance-forgetting trade-off problem, arguing that PiSSA forgets more as it fine-tunes the main principal components of a pre-trained model, which contain the main information, whereas last components contain long-tail or complementary information (Wang et al., 2024a). Differently from PiSSA and MiLoRA, we investigate intermediate components, under the assumption that both main and long-tail information needs to be preserved, especially in image classification applications. As we show in Figure 1, this assumption is confirmed by our study, where we see a U-shaped forgetting curve spanning over the principal components, and suggesting that fine-tuning intermediate components leads to inferior forgetting.

Understanding and addressing these trade-offs is crucial, especially for deploying foundation models in safety-critical (Pham & Sun, 2024), continual learning (Wang et al., 2024b; Verwimp et al., 2023), or multi-task (Vandenbende et al., 2021; Zhang & Yang, 2021; Quercia et al., 2025b) settings where the ability to adapt without sacrificing pre-trained

knowledge is vital (Kirkpatrick et al., 2017; Rahimi et al., 2023).

In this paper, we offer a systematic analysis of performance-forgetting trade-offs across a variety of LoRA variants. We characterize differences between PiSSA and MiLoRA, and propose a better initialization strategy based on intermediate principal components. In addition, we offer insights that guide the design of more robust PEFT learning strategies for improved stability-plasticity balance.

2. Related Work

The rapid scaling of foundation models with billions of parameters has transformed AI capabilities across Natural Language Processing and Computer Vision (Brown et al., 2020; Kaplan et al., 2020). However, full fine-tuning of these models remains computationally expensive, requiring extensive GPU memory and storage for each task adaptation (Houlsby et al., 2019).

Parameter-Efficient Fine-Tuning (PEFT) addresses this challenge by updating only a small fraction of parameters. LoRA (Hu et al., 2021) constrains weight updates to low-rank matrices, achieving comparable performance to full fine-tuning with a smaller percentage of parameters while preserving more of the pre-trained knowledge. Biderman et al. (Biderman et al., 2024) note that “LoRA learns less and forgets less,” highlighting its advantages in knowledge preservation, yet subsequent variants like DoRA (Liu et al., 2024) enhance adaptation by decomposing weights into magnitude and direction components. Similarly, PiSSA (Meng et al., 2024) and MiLoRA (Wang et al., 2024a) propose to initialize LoRA modules using main and minor principal components of the target pre-trained model, respectively, for enhanced efficiency on one hand, and for knowledge preservation on the other hand. In parallel, variants like VeRA (Kopczko et al., 2023) and 1LoRA (Quercia et al., 2025a) further minimize trainable parameters, with VeRA employing shared random matrices and layer-specific scaling vectors, and 1LoRA consolidating to a single trainable vector per module. Other LoRA variants dynamically prune less important ranks during training (AdaLoRA (Zhang et al., 2023)), or combine LoRA with 4-bit quantization for memory savings (QLoRA (Dettmers et al., 2023)). Lastly, other PEFT methods include BitFit (Zaken et al., 2021), which achieves extreme efficiency by tuning only bias terms, and DiffFit (Xie et al., 2023), which specializes in diffusion model adaptation.

3. Learning and forgetting

Pre-training large models requires prohibitive computational costs—often millions of GPU hours and billions in infrastructure. Consequently, adapting foundational models has

emerged as the practical strategy for downstream specialization. Given this reality, along with impending data scarcity where most available data has already been consumed by prior models, **continual fine-tuning** of pre-trained models on newly available data while preserving prior knowledge will become increasingly critical.

Recent approaches attempt to address this performance-forgetting trade-off through targeted low-rank updates (Hu et al., 2021): these methods constrain fine-tuning updates to a low-dimensional subspace by factorizing weight changes as the product of two low-rank matrices A and B as $\Delta W = AB$ ($A \in \mathbb{R}^{m \times r}$, $B \in \mathbb{R}^{r \times n}$, $r \ll \min(m, n)$), drastically reducing the number of trainable parameters while preserving expressive power. Rather than updating all model weights directly, only these compact low-rank factors are optimized, enabling efficient adaptation with minimal interference to pre-trained knowledge.

In this paper, we consider LoRA methods that do not alter the rank dramatically, and in particular we focus on principal-component-based initialization methods like PiSSA (Meng et al., 2024) and MiLoRA (Wang et al., 2024a), studying their differences and proposing a better alternative in terms of performance-forgetting trade-offs.

Catastrophic forgetting remains a critical limitation. While PEFT methods reduce resource demands, they often exhibit performance-forgetting trade-offs, particularly in continual learning (Kirkpatrick et al., 2017). Adaptive rank allocation (Zhang et al., 2023) and regularization strategies (Durgapal et al., 2023) show promise dynamically adjusting low-rank dimensions to balance expressivity and stability and penalizing deviations in critical subspaces, but systematic comparisons for principal components-based LoRA initialization methods are missing. In particular in-depth analyses of components and their effect on performance-forgetting have not yet been provided.

3.1. Choosing principal components

Unlike prior work focusing on isolated methods, we provide comprehensive analysis of the performance-forgetting dynamics across LoRA variants of similar rank, quantifying stability-plasticity trade-offs to guide robust PEFT design for continual learning.

PiSSA (Meng et al., 2024) leverages the intuition that the largest principal components of weight matrices capture the most expressive directions for new task performance. By selectively fine-tuning only these high-magnitude singular directions—while leaving smaller components frozen—it maximizes downstream adaptation capacity without broadly disrupting the model’s geometry. Conversely, MiLoRA (Wang et al., 2024a) exploits the hypothesis that the smallest principal components repre-

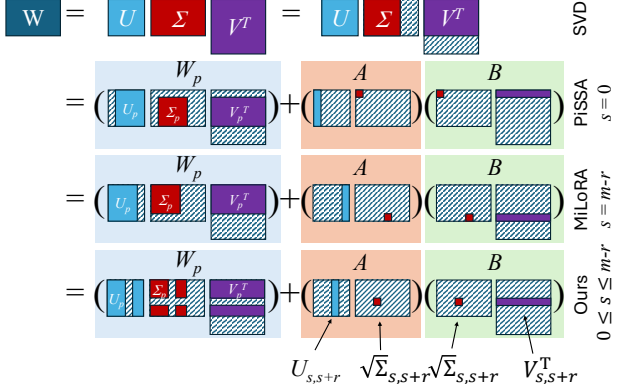


Figure 2. PiSSA, MiLoRA and our proposed approach.

sent task-orthogonal subspaces minimally utilized by prior training. Targeting these low-magnitude directions for fine-tuning minimizes interference with pre-trained representations while still providing sufficient expressivity for new tasks, achieving a principled forgetting-performance trade-off through spectral separation. Ideally, methods should optimize new task accuracy while preserving prior knowledge; however, we empirically demonstrate several fine-tuning scenarios where neither PiSSA nor MiLoRA achieve optimal performance-forgetting trade-offs. For this reason, we propose to fine-tune intermediate principal components, rather than the extremes.

We summarize PiSSA and MiLoRA in Figure 2, highlighting our proposed method that recommends fine-tuning intermediate components, based on our analysis and empirical findings.

3.2. Approach

Let W be a pre-trained $m \times n$ matrix, and $W = U\Sigma V^T$ its Singular Value Decomposition (SVD), where U and Σ are $m \times m$ and V^T is $m \times n$. We denote the considered matrix slices as $U_{s,s+r}$, $\Sigma_{s,s+r}$ and $V_{s,s+r}^T$, where s is the starting component and r is the rank. Therefore the decomposed matrix can be represented as $U = U_p + U_{s,s+r}$, $\Sigma = \Sigma_p + \Sigma_{s,s+r}$ and $V = V_p + V_{s,s+r}$. For example, the diagonal matrix is the sum of the following matrices

$$\Sigma_{s,s+r} = \text{diag}(0, \dots, 0, \sigma_s, \dots, \sigma_{s+r-1}, 0, \dots, 0)$$

$$\Sigma_p = \text{diag}(\sigma_0, \dots, \sigma_{s-1}, 0, \dots, 0, \sigma_{s+r}, \dots, \sigma_m)$$

We can then define the LoRA (Hu et al., 2021) matrices as

$$A = U_{s,s+r} \Sigma_{s,s+r}^{1/2} \quad \text{and} \quad B = \Sigma_{s,s+r}^{1/2} V_{s,s+r}^T \quad (1)$$

and the forward pass as

$$Y = X(W_p + \Delta W) = X(W_p + AB) \quad (2)$$

where X represents the input dataset and $W_p = W - U_{s,s+r}\Sigma_{s,s+r}V_{s,s+r}^T$ be the residual pre-trained matrix, which will be frozen during fine-tuning.

Note that this is a generalization of PiSSA (Meng et al., 2024) and MiLoRA (Wang et al., 2024a), where the former can be achieved with $s = 0$ and the latter with $s = m - r$.

3.3. Component analysis

We present an in-depth analysis investigating why extreme principal components exhibit higher susceptibility to catastrophic forgetting under extended fine-tuning or high learning rates. We further show that prolonged training exacerbates this phenomenon. Thus, we derive the conditions under which extreme principal components (at both spectrum ends, corresponding to PiSSA (Meng et al., 2024) and MiLoRA (Wang et al., 2024a)) undergo destabilizing dynamics during sequential task adaptation. Our analysis reveals how fine-tuning principal components at the extremes leads to higher damage to the main singular values, confirmed empirically as non-monotonic forgetting behavior across the singular value spectrum (Section 4). We first examine these dynamics in parameter space before analyzing their implications in feature space.

3.3.1. PARAMETER SPACE

Let W_0 and $W_{s,s+r}$ be the weight matrices of the considered pre-trained model before and after fine-tuning of components between s and $s+r$. To study the forgetting behavior depending on which components are fine-tuned, we analyze the changes to the parameters after fine-tuning in principal component space. In practice, we compute the SVD of the original weight matrix W_0

$$W_0 = U_{W_0} \Sigma_{W_0} V_{W_0}^T \quad (3)$$

and then we project the fine-tuned weight matrix $W_{s,s+r}$ into its coordinate system

$$\Sigma_{W_{s,s+r}} = U_{W_0}^T W_{s,s+r} V_{W_0} \quad (4)$$

where $\Sigma_{W_{s,s+r}}$ corresponds to Σ_{W_0} after fine-tuning. We denote the changes as

$$\Delta \Sigma_W = |\Sigma_{W_0} - \Sigma_{W_{s,s+r}}|. \quad (5)$$

We denote the diagonal and off-diagonal of $\Delta \Sigma_W$ by

$$\text{diag}(\Delta \Sigma_W) = (\Delta \Sigma_{W11}, \dots, \Delta \Sigma_{Wnn}) \quad (6)$$

and

$$\begin{aligned} \text{offdiag}(\Delta \Sigma_W) &= \Delta \Sigma_W - \text{diag}(\Delta \Sigma_W) \\ &= (\Delta \Sigma_{Wij})_{i,j=1}^n \quad \text{with } i \neq j. \end{aligned} \quad (7)$$

respectively. By this, we disentangle the changes in principal values (Eq. 6) from those in principal directions within

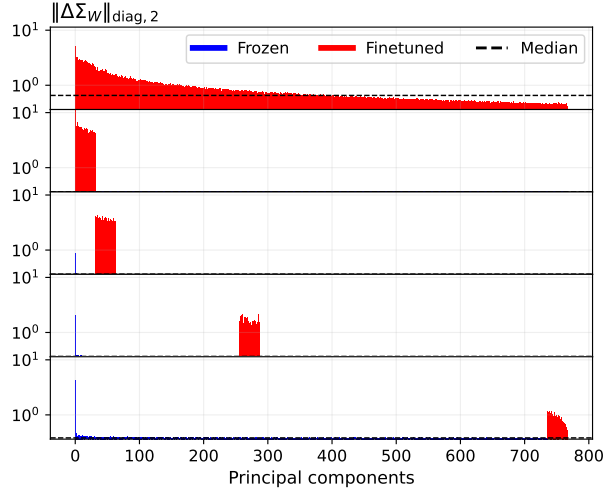


Figure 3. (ImageNet1k → Caltech101) Changes to the diagonal in parameter space, $\text{diag}(\Delta \Sigma_W)$, see Eq. 6. We show the element-wise norm.

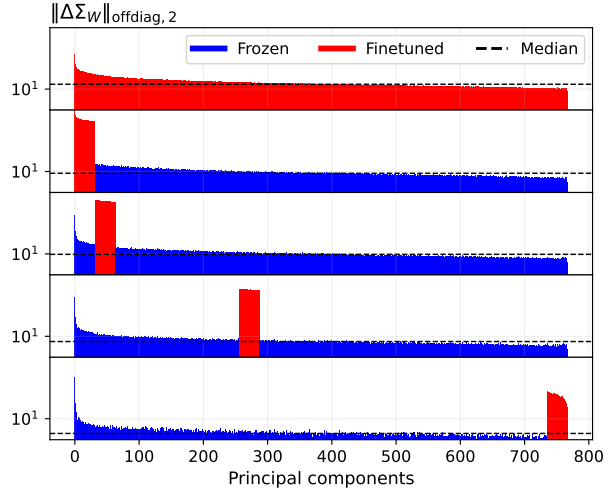


Figure 4. (ImageNet1k → Caltech101) Changes to the off-diagonal in parameter space, $\text{offdiag}(\Delta \Sigma_W)$, see Eq. 7. We show the column-wise norm $\|\text{offdiag}(\Delta \Sigma_W)_i\|_2$.

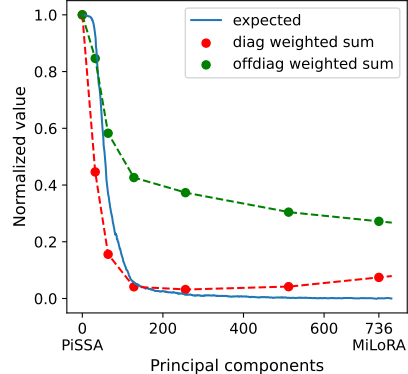


Figure 5. Normalized expected forgetting, scaled diagonal (red) and off-diagonal (green) sum of changes in parameter space.

the SVD of weight update matrices, and relate this to the observed empirical behavior in the experiments (Sect. 4). This decomposition isolates the scaling of principal components from their directional shifts (off-diagonal changes), enabling precise attribution of behavioral changes to specific subspaces of the parameter space. By analyzing these distinct contributions separately, our approach reveals how fine-tuning modifies the geometry of weight updates across different principal components. This framework facilitates a deeper analysis of forgetting phenomena by linking the observed U-shaped forgetting curve to the changes in principal components.

In particular, we show the analysis corresponding to results in Figure 1. Figures 3 and 4 show the diagonal and off-diagonal L2 norms of the models in the considered experiment. From top to bottom, we display fine-tuning all parameters, fine-tuning components 0-32 (PiSSA), 32-64, 256-288, and 736-768 (MiLoRA). We observe from the figures, that fine-tuning in a certain low-rank region changes the respective singular values most, as expected. However, also other 'frozen' components are changed due to rotation of the 'hot' low rank subspace. Specifically, it emerges that fine-tuning the extremes (PiSSA or MiLoRA) also leads to higher changes to the very first principal component, and subsequent ones, suggesting that main information from the previous task might be damaged more.

In Figure 5 we show a summary of the previous figures, by computing the sum over the components, weighted by their 'expected' contribution p to forgetting. To generate p_i , we zero out the i -th principal component of the pre-trained model, evaluate on the prior data, and compute the resulting forgetting value f_i . Finally, we normalize $p_i = f_i / \max_j(f_j)$. p is shown as blue line. We then compute the weighted sums $\sum_i p_i \cdot \|\text{diag}(\Delta\Sigma_W)_{ii}\|_2$ (red line) and $\sum_i p_i \cdot \|\text{offdiag}(\Delta\Sigma_W)_{ii}\|_2$ (green line) for the diagonal and off-diagonal of $\Delta\Sigma_W$, respectively, see Eqs. 6 and 7. The figure highlights that in contrast with the 'expected' behaviour (p , blue line), where forgetting decreases monotonically with increasing principal components, the weighted diagonal (red line) forms a soft U-shape. This indicates that fine-tuning components at the extremes leads to higher damage in the pre-trained model. We show the changes in feature space in the next subsection.

3.3.2. FEATURE SPACE

Let W_0 and $W_{s,s+r}$ be the weight matrices of the considered pre-trained model before and after fine-tuning of components between s and $s+r$. And let X_0 be a small, random but fixed subset of the data used to pre-train W_0 , and let

$$Y_0 = X_0 W_0 \quad (8)$$

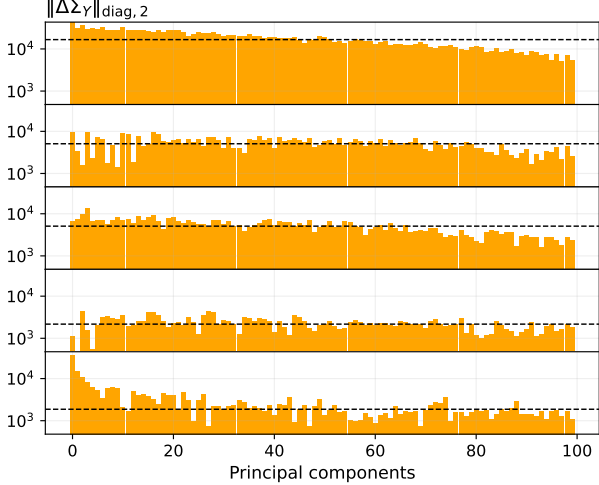


Figure 6. (ImageNet1k → Caltech101) Changes to the diagonal in feature space, $\text{diag}(\Delta\Sigma_Y)$, see Eq. 11. We show the element-wise norm.

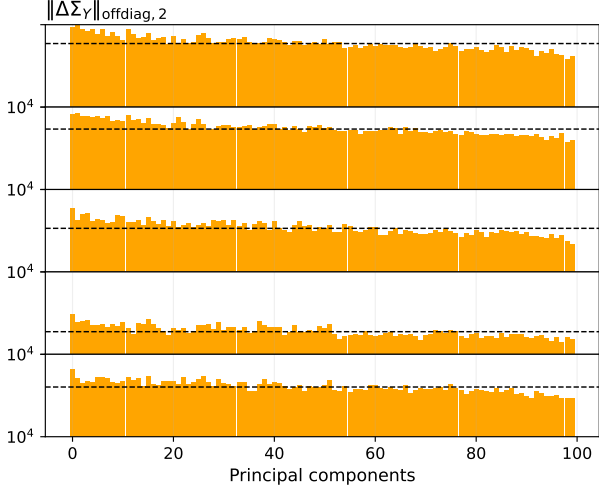


Figure 7. (ImageNet1k → Caltech101) Changes to the diagonal in feature space, $\text{offdiag}(\Delta\Sigma_Y)$. We show the column-wise norm $\|\text{offdiag}(\Delta\Sigma_Y)_{ii}\|_2$

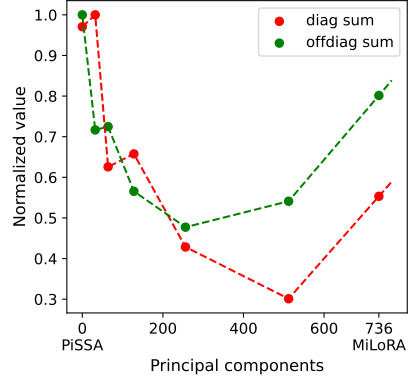


Figure 8. Normalized expected forgetting, scaled diagonal (red) and off-diagonal (green) sum of changes in feature space.

be the outputs of each considered layer in model W_0 for inputs X_0 . In this study we analyze the changes in feature space after fine-tuning. To do so, we compute the SVD

$$Y_0 = U_{Y_0} \Sigma_{Y_0} V_{Y_0}^T \quad (9)$$

and then we project the outputs of fine-tuned weight matrix $Y_{s,s+r} = X_0 W_{s,s+r}$ into its coordinate system as follows

$$\Sigma_{Y_{s,s+r}} = U_{Y_0}^T Y_{s,s+r} V_{Y_0} \quad (10)$$

where $\Sigma_{Y_{s,s+r}}$. We denote the changes in feature space as

$$\Delta \Sigma_Y = |\Sigma_{Y_0} - \Sigma_{Y_{s,s+r}}|. \quad (11)$$

Lastly, we denote the diagonal and off-diagonal of $\Delta \Sigma_Y$ as $\text{diag}(\Delta \Sigma_Y)$ and $\text{offdiag}(\Delta \Sigma_Y)$, respectively. Here, we disentangle the changes in principal values from those in principal directions, as done for the parameter space.

Figures 6 and 7 show the changes in feature space for X_0 being a subset of 100 samples, displaying the diagonal and off-diagonal L2 norms of the models in the considered experiment. These figures confirm our previous analysis, showing that fine-tuning all parameters and extreme components (first 2 rows and last one) lead to higher changes in feature space, whereas fine-tuning intermediate components lead to less changes.

This is summarized in Figure 8, where we show the sum over the components, together with the ‘expected’ distribution, where we see that changes in feature space form a U-shape, both in diagonal and off-diagonal. Please note that these analyses are made on single models, whereas in Figure 1 we report mean and standard deviation.

We observe, that the shallower U-shape in parameter space translates to a more pronounced U-shape in feature space.

4. Experiments

We conduct an extensive empirical study with two main focus points: (i) using our proposed analysis, we study the impact of the principal components used, and of the training time on forgetting and accuracy, and (ii) based on our findings, we propose a balanced trade-off method leveraging intermediate principle components. For the latter, we assess the effectiveness and robustness of the proposed method across both vision and language domains, comparing it against recent LoRA methods with fixed rank and similar number of parameters for comparability: LoRA (Hu et al., 2021), DoRA (Liu et al., 2024), PiSSA (Meng et al., 2024), MiLoRA (Wang et al., 2024a). Our study covers a broad spectrum of Image Classification cases, including datasets of varying scale, complexity, and number of classes. In addition, we systematically evaluate on diverse NLP tasks spanning mathematical reasoning, python coding and common sense tasks, thereby analyzing behavior under heterogeneous data distributions and task formats.

4.1. Image Classification

We examine whether our findings generalize to other image classification datasets. We evaluate the impact on performance and forgetting of fine-tuning different principal component ranges, with starting points s (0, 4, 16, 32, 64, 128, 256, 512, 736) with rank $r = 32$, where $s = 0$ is PiSSA (Meng et al., 2024) and $s = 736$ is MiLoRA (Wang et al., 2024a). We fine-tune an ImageNet1k pre-trained ViT-B on a variety of image classification datasets: CIFAR10, CIFAR100, DTD, Caltech101, Caltech256, Food101, Oxford Pets, Oxford Flowers 102, Stanford Cars, Stanford Dogs, and FGVC Aircraft. In these experiments, we compute forgetting as absolute difference of accuracies (before and after fine-tuning). Note that this forgetting is correlated to the forgetting as computed in (Wang et al., 2024a; Kalajdzievski, 2024). Training details are reported in Appendix A.1.

From Figure 9 we observe that forgetting exhibits a characteristic U-shaped curve when models are fine-tuned to high accuracy on a new task, i.e. long enough to fit it properly or to over-fit it. The longer the fine-tuning duration on the new task, the more pronounced this U-shape becomes. This pattern indicates that **both the highest and lowest principal components are particularly susceptible to catastrophic forgetting under extended fine-tuning**. Therefore the trade-off accuracy-forgetting is dominated by the forgetting, and the best value shows up “in the middle”, i.e. when fine-tuning intermediate principal components, as shown by the sum of accuracies reported in Figure 9 (right-most).

We report experiments on additional datasets in Table 1, where the observed behaviour is confirmed, with more or less pronounced U-shapes. In summary, when a model is trained for long-enough, the accuracy on the new task seems to plateau and reach approximately the same value for each starting point, whereas the forgetting forms a U-shape, where extreme values are higher than intermediate ones, leading to intermediate components having better performance-forgetting trade-offs. This confirms the analysis of the U-shape phenomenon provided in Section 3.3.

In Table 1, we report the result for the best intermediate component range and the result achieved when fine-tuning the components between $s = 256$ and $s + r = 288$; in some cases this coincides with the best, whereas in other cases it is very close to it in terms of performance, suggesting that any value other than the extremes leads to an improved trade-off.

4.2. Natural Language Processing Tasks

Here, we study whether our findings generalize to NLP tasks. We fine-tune a pre-trained LLaMA-2 model on three NLP tasks: mathematical reasoning, python coding and common

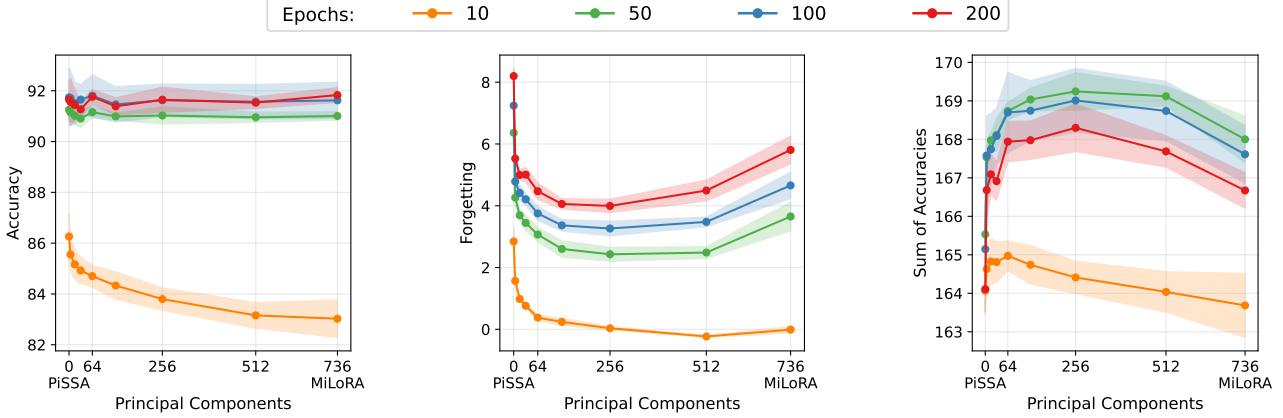


Figure 9. (ImageNet1k \rightarrow Caltech101) Results of fine-tuning an ImageNet1k pre-trained ViT-Base to Caltech101, using different principal component slices with starting points s (horizontal axis) and rank 32. From left to right, accuracy of Caltech101, forgetting of ImageNet1k, and sum of accuracies of Caltech101 and ImageNet1k at the end of fine-tuning.

Table 1. Image Classification. Sum of accuracies of Imagenet1k and various finetuned classification datasets, after fine-tuning. Highest mean of 4 independent runs, among evaluations computed from epoch 50. Values achieved by $s = 256$ are close to those achieved by the best tested s . We highlight **best** and second best.

Methods	CIFAR10	CIFAR100	DTD	Caltech101	Caltech256	Food101
Full	175.53 ± 0.63	167.11 ± 0.49	149.57 ± 2.13	161.45 ± 0.57	160.02 ± 1.24	165.43 ± 0.26
LoRA	177.77 ± 0.16	168.70 ± 0.33	142.60 ± 0.35	159.77 ± 0.46	163.45 ± 0.90	166.67 ± 0.22
DoRA	177.73 ± 0.14	168.65 ± 0.39	142.58 ± 0.40	159.78 ± 0.45	163.45 ± 0.78	166.64 ± 0.18
PiSSA	176.76 ± 0.48	169.23 ± 0.25	149.06 ± 0.68	165.53 ± 0.74	167.12 ± 0.70	167.64 ± 0.61
Ours (256)	179.13 ± 0.15	171.93 ± 0.14	155.07 ± 0.71	169.25 ± 0.48	171.18 ± 0.30	169.47 ± 0.17
Ours (Best)	179.24 ± 0.09	171.93 ± 0.14	155.27 ± 0.95	169.25 ± 0.48	171.18 ± 0.30	169.62 ± 0.19
MiLoRA	179.16 ± 0.08	171.27 ± 0.10	152.85 ± 0.72	168.00 ± 0.60	169.25 ± 0.37	168.86 ± 0.13
Methods	O. Pets	O. Flowers102	S. Cars	S. Dogs	FGVC Aircraft	Average
Full	168.27 ± 0.71	176.72 ± 0.07	155.34 ± 0.33	165.53 ± 0.33	148.23 ± 0.36	163.02 ± 0.65
LoRA	168.18 ± 0.65	176.14 ± 0.29	148.26 ± 0.54	170.30 ± 0.20	138.57 ± 1.73	161.86 ± 0.53
DoRA	168.10 ± 0.65	176.17 ± 0.26	148.33 ± 0.45	170.27 ± 0.27	139.03 ± 1.61	161.88 ± 0.51
PiSSA	170.27 ± 0.21	177.94 ± 0.28	154.51 ± 0.56	169.76 ± 0.19	145.93 ± 0.59	164.89 ± 0.48
Ours (256)	172.70 ± 0.18	179.47 ± 0.15	158.26 ± 0.52	171.13 ± 0.07	146.52 ± 0.55	167.65 ± 0.31
Ours (Best)	172.85 ± 0.21	179.47 ± 0.15	158.51 ± 0.24	171.41 ± 0.11	147.80 ± 0.84	167.87 ± 0.34
MiLoRA	172.05 ± 0.50	179.27 ± 0.20	155.55 ± 0.49	171.41 ± 0.11	144.01 ± 0.39	166.52 ± 0.34

sense. We study the impact of fine-tuning components at the extremes (PiSSA and MiLoRA) and intermediate ones, using our generalized method. We use different starting points s (0, 1024, 2048, 3072, 3968) with rank $r = 128$, where $s = 0$ is PiSSA (Meng et al., 2024) and $s = 3968$ is MiLoRA (Wang et al., 2024a). We benchmark all methods with 3 different training setups: the one used in PiSSA (Meng et al., 2024), the one suggested by MiLoRA (Wang et al., 2024a), and ours, which adapts PiSSA’s one to the highest learning rate possible. We notice that MiLoRA proposes various changes to PiSSA’s setup, whereas we investigate the impact of the learning rate only. In these experiments, we compute forgetting as in (Wang et al., 2024a; Kalajdzievski, 2024), with a soft cross-entropy loss which uses tokens predicted by the model before fine-tuning as targets and tokens predicted by the model after fine-tuning as

predictions. Training details are reported in Appendix A.2.

In Figure 10 we report average accuracy and forgetting results for fine-tuning LLaMA-2 on python coding datasets using the described training setups, showing that PiSSA excels in PiSSA’s setup, MiLoRA is better than PiSSA in MiLoRA’s setup, and our method is even better than MiLoRA. Most importantly, by modifying PiSSA’s setup to a higher learning rate, we observe that forgetting forms the previously observed U-shape, and accuracy the opposite, i.e., a reversed U-shape, confirming intermediate components as best performance-forgetting trade-offs. Additionally, when using a high learning rate, we see that intermediate components are more robust, whereas extremes can more easily lead to exploding gradients, and consequently high damage to the prior knowledge in the original model. Lastly, our

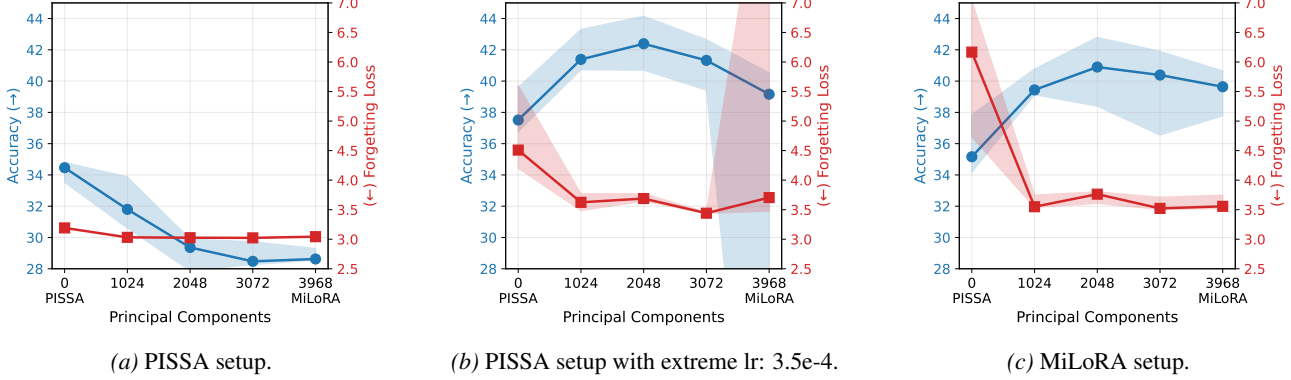


Figure 10. Python coding results with LLaMA-2 7b. We report median and min/max. Outlier values correspond to runs with exploding gradients. Training details in Table S1.

Table 2. Python coding results with LLaMA-2 7b. We report mean and standard deviation over 4 independent runs. High standard deviations include runs with exploding gradients. We highlight **best** and second best.

Methods	Human-eval	Human-eval+	MBPP	MBPP+	Average (↑)	Forgetting (↓)
PiSSA	31.23 ± 2.36	28.98 ± 2.09	42.25 ± 1.71	34.80 ± 1.65	34.31 ± 0.56	3.19 ± 0.00
PiSSA (ours)	38.73 ± 1.91	35.23 ± 2.02	42.08 ± 1.08	35.38 ± 1.16	37.85 ± 1.35	4.71 ± 0.64
Ours (1024)	43.92 ± 2.13	39.32 ± 2.09	44.65 ± 0.67	38.90 ± 0.48	41.70 ± 1.17	3.63 ± 0.12
Ours (2048)	44.22 ± 4.03	40.10 ± 4.17	46.48 ± 1.24	38.82 ± 1.07	42.41 ± 1.65	3.70 ± 0.06
Ours (3072)	43.30 ± 4.02	38.12 ± 3.34	45.67 ± 1.92	37.62 ± 0.69	41.18 ± 1.37	3.44 ± 0.01
MiLoRA (ours)	30.97 ± 20.65	27.45 ± 18.32	32.73 ± 21.92	27.70 ± 18.47	29.71 ± 19.83	5.25 ± 3.25
MiLoRA	39.02 ± 1.81	35.83 ± 1.77	45.17 ± 1.50	37.68 ± 1.76	39.42 ± 1.40	3.59 ± 0.10

setup leads to superior results in terms of accuracy, when compared to the other setups.

Tables 2, S2 and S3 display the results for python coding, mathematical reasoning and common sense datasets. Here, we see that we improve the performance-forgetting trade-off over both PISSA and MiLoRA by fine-tuning intermediate components and increasing the learning rate to “the highest stable possible”. This is possible as intermediate components interfere less with the main components, as shown in Sec. 3.3. As a result, intermediate components are also more robust to higher learning rate settings than extreme components, consistently leading to better results.

5. Conclusion

Low-Rank Adaptation (LoRA) has become key for adapting large pre-trained models to downstream tasks. However, they face a fundamental challenge: achieving strong task-specific performance while avoiding catastrophic forgetting of pre-trained knowledge. Existing approaches offer inconsistent guidance on how to make this trade-off.

In this paper, we offer the first principled study into principle component based initialization methods for low-rank adaptation. We offer a new analysis approach that allows us to study the impact of components used for fine-tuning and of training duration. We propose a method that leverages

intermediate components as a means of achieving superior trade-offs in learning and forgetting.

We empirically demonstrate when a model is fine-tuned long enough, its accuracy plateaus around a maximum value for any rank, whereas the forgetting forms a U-shape, where models fine-tuned using intermediate components show the least forgetting. This suggests that components at the extremes are more prone to forget than intermediate ones.

We therefore propose to make use of intermediate components for better trading off accuracy and forgetting. Our findings pave the way for designing targeted interventions—such as selective rank pruning or direction-constrained updates—that mitigate catastrophic forgetting while preserving downstream performance, ultimately advancing the reliability of continual learning in large-scale models.

Acknowledgments

The authors gratefully acknowledge the Gauss Centre for Supercomputing e.V. (www.gauss-centre.eu) for funding this project by providing computing time through the John von Neumann Institute for Computing (NIC) on the GCS Supercomputer JUWELS (Kesselheim et al., 2021) at Jülich Supercomputing Centre (JSC).

References

Biderman, D., Portes, J., Ortiz, J. J. G., Paul, M., Greengard, P., Jennings, C., King, D., Havens, S., Chiley, V., Frankle, J., et al. Lora learns less and forgets less. *arXiv preprint arXiv:2405.09673*, 2024.

Brown, T. B., Mann, B., Ryder, N., Subbiah, M., Kaplan, J., Dhariwal, P., Neelakantan, A., Shyam, P., Sastry, G., Askell, A., et al. Language models are few-shot learners. *Advances in Neural Information Processing Systems*, 33: 1877–1901, 2020.

Chen, M.-W., Lyu, L., Chen, D., and Stephens, C. R. Gpt-oriented pretraining for large language models. *arXiv preprint arXiv:2204.00234*, 2022.

Dai, Z., Wen, Y., and Zhang, Z. Alpaca: Instruction-following llm fine-tuning with minimal human supervision. *arXiv preprint arXiv:2305.09554*, 2023.

Dettmers, T., Pagnoni, A., Holtzman, A., and Zettlemoyer, L. Qlora: Efficient finetuning of quantized llms. *Advances in neural information processing systems*, 36:10088–10115, 2023.

Durgapal, N., Ba, J., and LeCun, Y. Regularization strategies for fine-tuning large language models. *Journal of Machine Learning Research*, 24:1–34, 2023.

Houlsby, N., Giurgiu, A., Jastrzebski, S., Morrone, J., De Laroussilhe, Q., Gesmundo, A., Attariyan, M., and Gelly, S. Parameter-efficient transfer learning for nlp. In *Proceedings of the 36th International Conference on Machine Learning*, volume 97, pp. 2790–2799, 2019.

Hu, E. J., Shen, Y., Wallis, P., Allen-Zhu, Z., Li, Y., Wang, S., Wang, L., and Chen, W. Lora: Low-rank adaptation of large language models. *arXiv preprint arXiv:2106.09685*, 2021.

Kalajdzievski, D. Scaling laws for forgetting when fine-tuning large language models. *arXiv preprint arXiv:2401.05605*, 2024.

Kaplan, J., McCandlish, S., Henighan, T., Brown, T. B., Chess, B., Child, R., Gray, S., Radford, A., Wu, J., and Amodei, D. Scaling laws for neural language models. *arXiv preprint arXiv:2001.08361*, 2020.

Kesselheim, S., Herten, A., Krajsek, K., Ebert, J., Jitsev, J., Cherti, M., Langguth, M., Gong, B., Stadtler, S., Mozafari, A., et al. Juwels booster—a supercomputer for large-scale ai research. In *International Conference on High Performance Computing*, pp. 453–468. Springer, 2021.

Kirkpatrick, J., Pascanu, R., Rabinowitz, N., Veness, J., Desjardins, G., Rusu, A. A., Milan, K., Quan, J., Ramalho, T., Grabska-Barwinska, A., et al. Overcoming catastrophic forgetting in neural networks. *Proceedings of the National Academy of Sciences*, 114(13):3521–3526, 2017.

Kopitzko, D. J., Blankevoort, T., and Asano, Y. M. Vera: Vector-based random matrix adaptation. *arXiv preprint arXiv:2310.11454*, 2023.

Liu, S.-Y., Wang, C.-Y., Yin, H., Molchanov, P., Wang, Y.-C. F., Cheng, K.-T., and Chen, M.-H. Dora: Weight-decomposed low-rank adaptation. *arXiv preprint arXiv:2402.09353*, 2024.

Meng, F., Wang, Z., and Zhang, M. Pissa: Principal singular values and singular vectors adaptation of large language models. *Advances in Neural Information Processing Systems*, 37:121038–121072, 2024.

Pham, L. H. and Sun, J. Certified continual learning for neural network regression. In *Proceedings of the 33rd ACM SIGSOFT International Symposium on Software Testing and Analysis*, pp. 806–818, 2024.

Quercia, A., Cao, Z., Bangun, A., Paul, R. D., Morrison, A., Assent, I., and Scharr, H. 1lora: Summation compression for very low-rank adaptation. *arXiv preprint arXiv:2503.08333*, 2025a.

Quercia, A., Yildiz, E., Cao, Z., Krajsek, K., Morrison, A., Assent, I., and Scharr, H. Enhancing monocular depth estimation with multi-source auxiliary tasks. In *2025 IEEE/CVF Winter Conference on Applications of Computer Vision (WACV)*, pp. 6435–6445. IEEE, 2025b.

Rahimi, J., Nguyen, A., Martinez, A., and Chen, L. Learning without forgetting via continual contrastive and generative replay. In *Proceedings of the 2023 Conference on Neural Information Processing Systems*, 2023.

Stickland, A. and Murray, I. Pass: Parameter-efficient architecture search in vision transformers. In *Proceedings of the 38th International Conference on Machine Learning*, volume 139, pp. 9914–9927, 2021.

Vandenhende, S., Georgoulis, S., Van Gansbeke, W., Proesmans, M., Dai, D., and Van Gool, L. Multi-task learning for dense prediction tasks: A survey. *IEEE transactions on pattern analysis and machine intelligence*, 44(7):3614–3633, 2021.

Verwimp, E., Aljundi, R., Ben-David, S., Bethge, M., Cossu, A., Gepperth, A., Hayes, T. L., Hüllermeier, E., Kanan, C., Kudithipudi, D., et al. Continual learning: Applications and the road forward. *arXiv preprint arXiv:2311.11908*, 2023.

Wang, H., Li, Y., Wang, S., Chen, G., and Chen, Y. Milora: Harnessing minor singular components for parameter-efficient llm finetuning. *arXiv preprint arXiv:2406.09044*, 2024a.

Wang, L., Zhang, X., Su, H., and Zhu, J. A comprehensive survey of continual learning: Theory, method and application. *IEEE transactions on pattern analysis and machine intelligence*, 46(8):5362–5383, 2024b.

Xie, E., Yao, L., Shi, H., Liu, Z., Zhou, D., Liu, Z., Li, J., and Li, Z. Diffit: Unlocking transferability of large diffusion models via simple parameter-efficient fine-tuning. *arXiv preprint arXiv:2304.06648*, 2023.

Zaken, E. B., Ravfogel, S., and Goldberg, Y. Bitfit: Simple parameter-efficient fine-tuning for transformer-based masked language-models. *arXiv preprint arXiv:2106.10199*, 2021.

Zhang, Q., Chen, M., Bukharin, A., Karampatziakis, N., He, P., Cheng, Y., Chen, W., and Zhao, T. Adalora: Adaptive budget allocation for parameter-efficient fine-tuning. *arXiv preprint arXiv:2303.10512*, 2023.

Zhang, Y. and Yang, Q. A survey on multi-task learning. *IEEE Transactions on Knowledge and Data Engineering*, 34(12):5586–5609, 2021.

Supplementary Material

A. Training details

A.1. Image Classification

We conduct all image classification experiments using a simple training procedure for ViT-B: rank $r = 32$, scaling factor $\alpha = 32$, AdamW optimizer (LR= 2×10^{-5} , weight decay=0.01), batch size 10, over 200 epochs. As starting components we use 0 (PiSSA), 32, 64, 128, 256, 512, 736 (MiLoRA).

A.2. NLP Tasks

For the NLP tasks we use 3 different training setups: PiSSA (Meng et al., 2024), MiLoRA (Wang et al., 2024a), and ours (i.e., PiSSA with higher learning rate). Configurations are reported in Table S1. As starting components we use: 0 (PiSSA), 1024, 2048, 3072, 3968 (MiLoRA).

Table S1. Hyperparameter configuration on the common-sense reasoning (ComR), math reasoning (MathR) and instruction-following (InsF) tasks.

Hyperparameters	PiSSA	Ours	MiLoRA
Rank r	128	128	64
α of PiSSA/MiLoRA	128	128	64
Dropout	—	—	0.05
Optimizer	AdamW	AdamW	AdamW
LR	Cosine	Cosine	Linear
LR Scheduler	2e-5	3.5e-4, 3e-4, 1e-4	3e-4
Batch size	128	128	16
Warmup ratio	0.03	0.03	—
Warmup steps	—	—	100
Epochs	3	3	3
Placement	query, key, value, output, gate, MLP up, MLP down	query, key, value, output, gate, MLP up, MLP down	query, key, value, MLP up, MLP down

B. Additional experiments

B.1. Image Classification

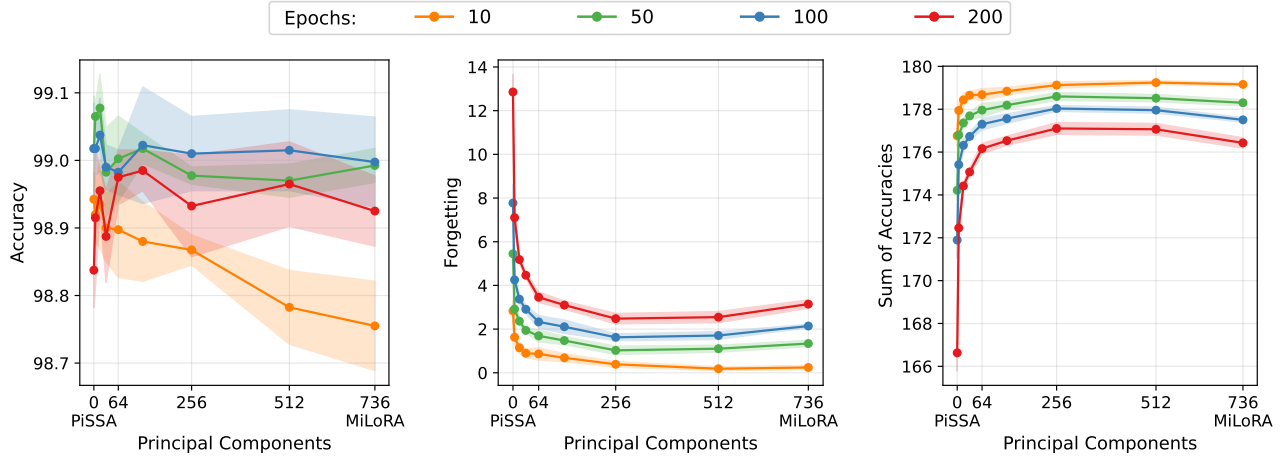


Figure 11. (ImageNet1k \rightarrow CIFAR10) Results of fine-tuning an ImageNet1k pre-trained ViT-Base to CIFAR10 using SPISSA with rank 32, using different starting points. From left to right, accuracy of CIFAR10, forgetting of ImageNet1k, and sum of accuracies of CIFAR10 and ImageNet1k at the end of fine-tuning.

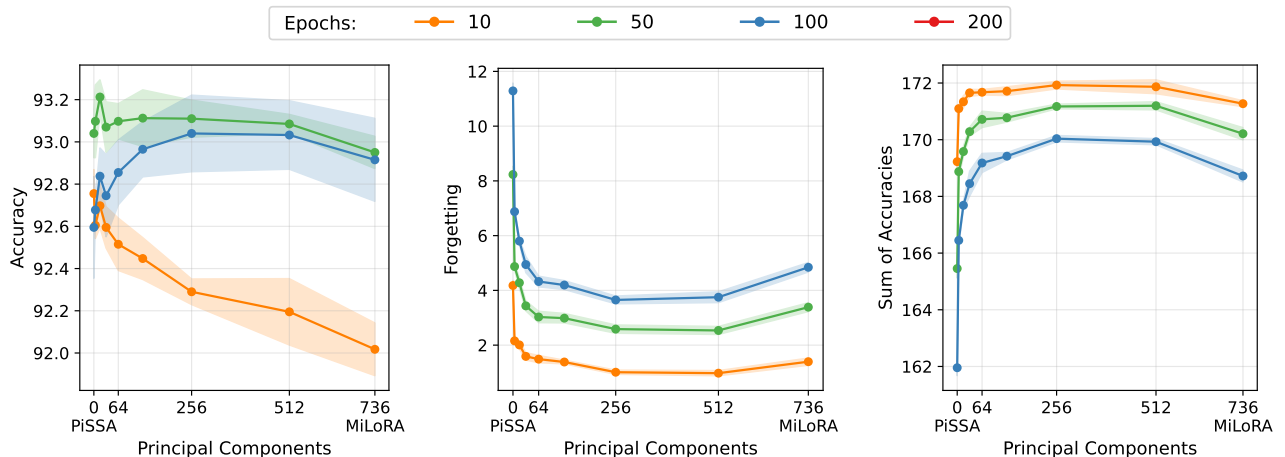


Figure 12. (ImageNet1k \rightarrow CIFAR100) Results of fine-tuning an ImageNet1k pre-trained ViT-Base to CIFAR100 using SPISSA with rank 32, using different starting points. From left to right, accuracy of CIFAR100, forgetting of ImageNet1k, and sum of accuracies of CIFAR100 and ImageNet1k at the end of fine-tuning.

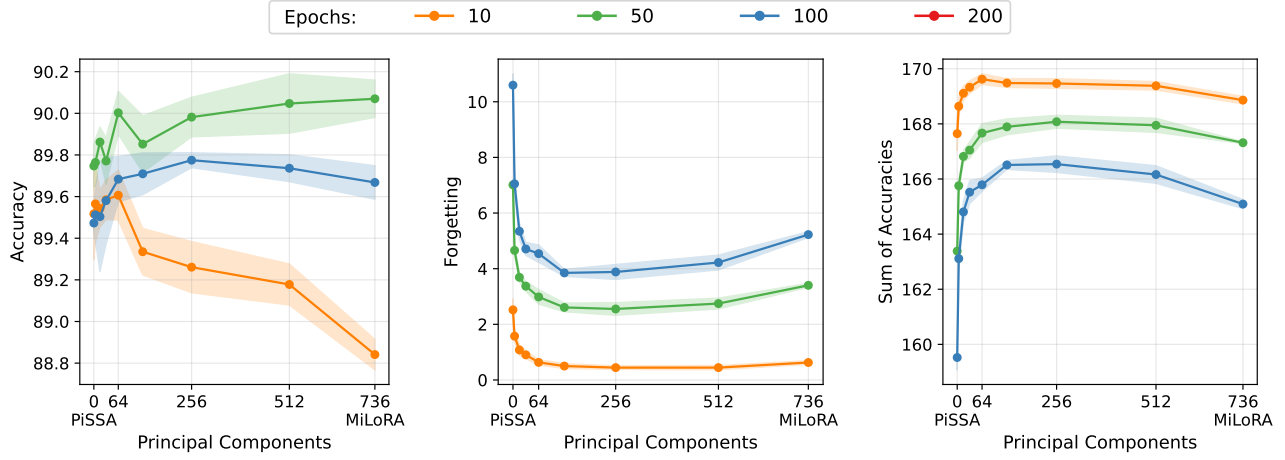


Figure 13. (ImageNet1k → Food101) Results of fine-tuning an ImageNet1k pre-trained ViT-Base to Food101 using SPISSA with rank 32, using different starting points. From left to right, accuracy of Food101, forgetting of ImageNet1k, and sum of accuracies of Food101 and ImageNet1k at the end of fine-tuning.

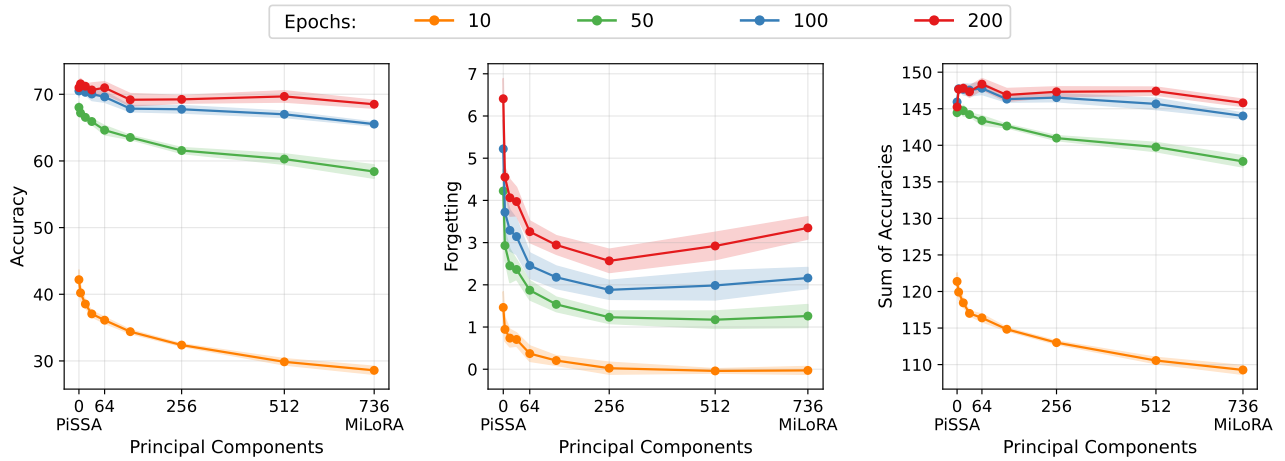


Figure 14. (ImageNet1k → FGVC Aircraft) Results of fine-tuning an ImageNet1k pre-trained ViT-Base to FGVC Aircraft using SPISSA with rank 32, using different starting points. From left to right, accuracy of FGVC Aircraft, forgetting of ImageNet1k, and sum of accuracies of FGVC Aircraft and ImageNet1k at the end of fine-tuning.

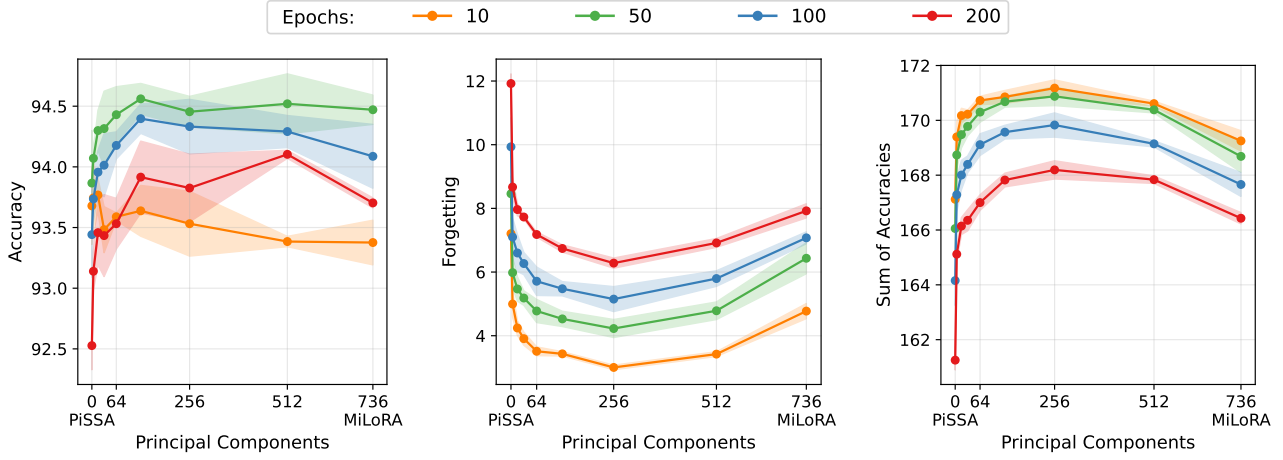


Figure 15. (ImageNet1k \rightarrow Caltech256) Results of fine-tuning an ImageNet1k pre-trained ViT-Base to Caltech256 using SPISSA with rank 32, using different starting points. From left to right, accuracy of Caltech256, forgetting of ImageNet1k, and sum of accuracies of Caltech256 and ImageNet1k at the end of fine-tuning.

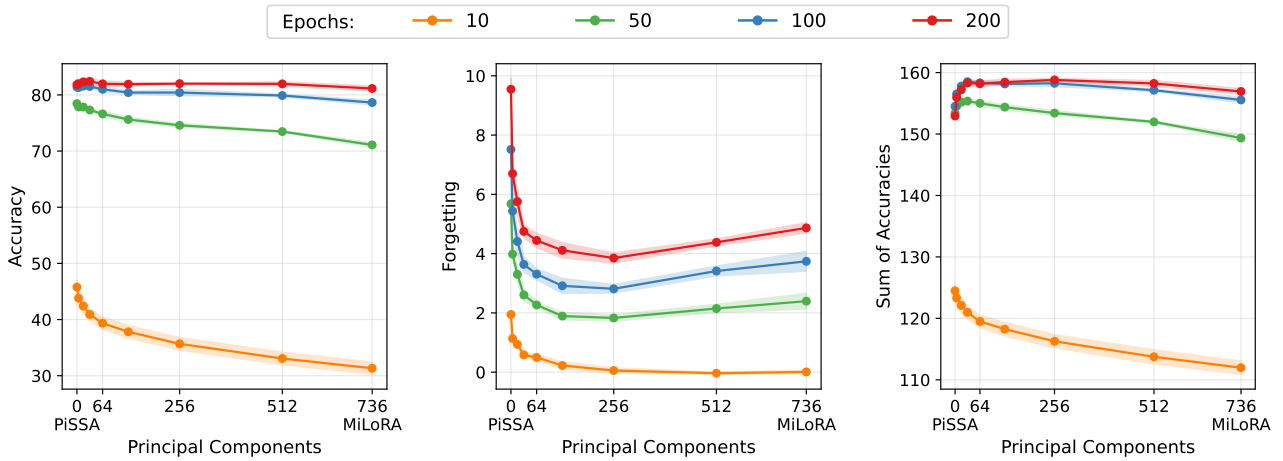


Figure 16. (ImageNet1k \rightarrow Stanford-Cars) Results of fine-tuning an ImageNet1k pre-trained ViT-Base to Stanford-Cars using SPISSA with rank 32, using different starting points. From left to right, accuracy of Stanford-Cars, forgetting of ImageNet1k, and sum of accuracies of Stanford-Cars and ImageNet1k at the end of fine-tuning.

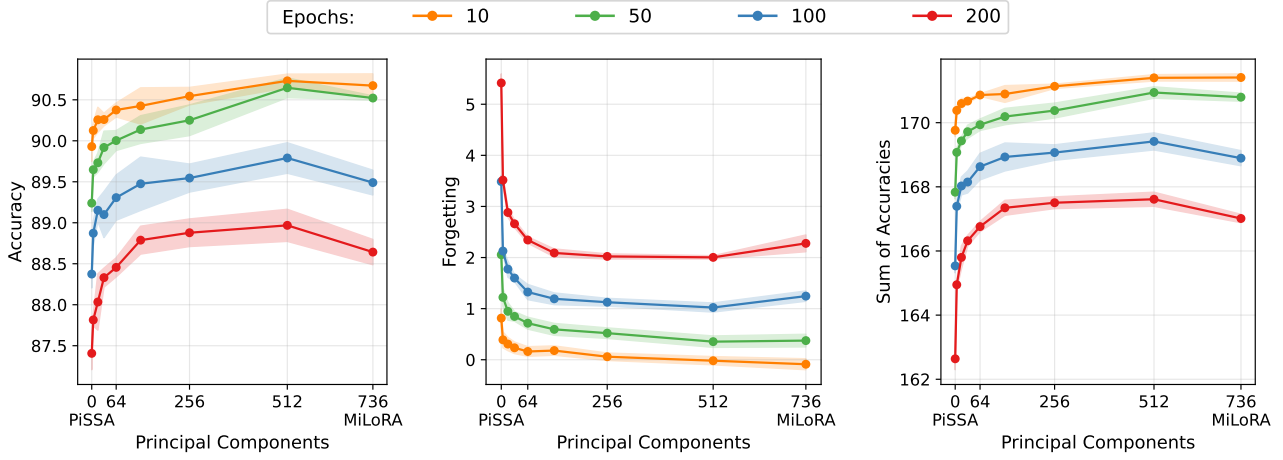


Figure 17. (ImageNet1k → Stanford-Dogs) Results of fine-tuning an ImageNet1k pre-trained ViT-Base to Stanford-Dogs using SPISSA with rank 32, using different starting points. From left to right, accuracy of Stanford-Dogs, forgetting of ImageNet1k, and sum of accuracies of Stanford-Dogs and ImageNet1k at the end of fine-tuning.

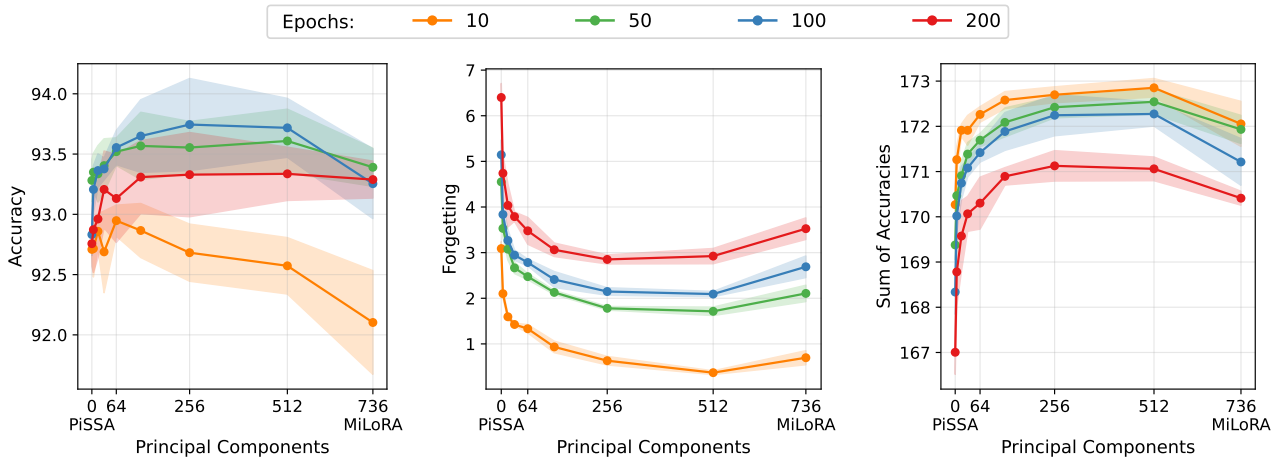


Figure 18. (ImageNet1k → Oxford Pets) Results of fine-tuning an ImageNet1k pre-trained ViT-Base to Oxford Pets using SPISSA with rank 32, using different starting points. From left to right, accuracy of Oxford Pets, forgetting of ImageNet1k, and sum of accuracies of Oxford Pets and ImageNet1k at the end of fine-tuning.

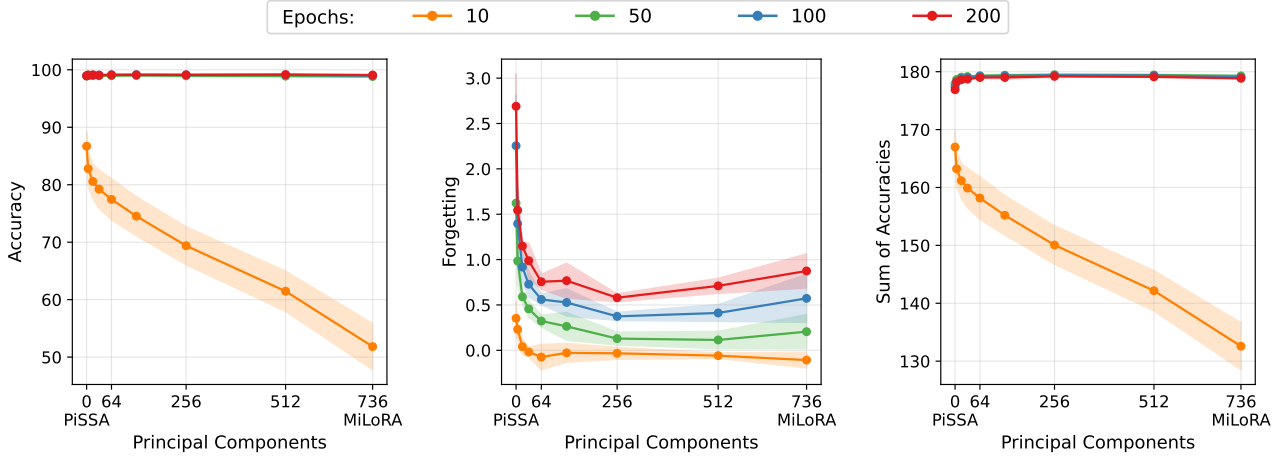


Figure 19. (ImageNet1k → Oxford Flowers102) Results of fine-tuning an ImageNet1k pre-trained ViT-Base to Oxford Flowers102 using SPISSA with rank 32, using different starting points. From left to right, accuracy of Oxford Flowers102, forgetting of ImageNet1k, and sum of accuracies of Oxford Flowers102 and ImageNet1k at the end of fine-tuning.

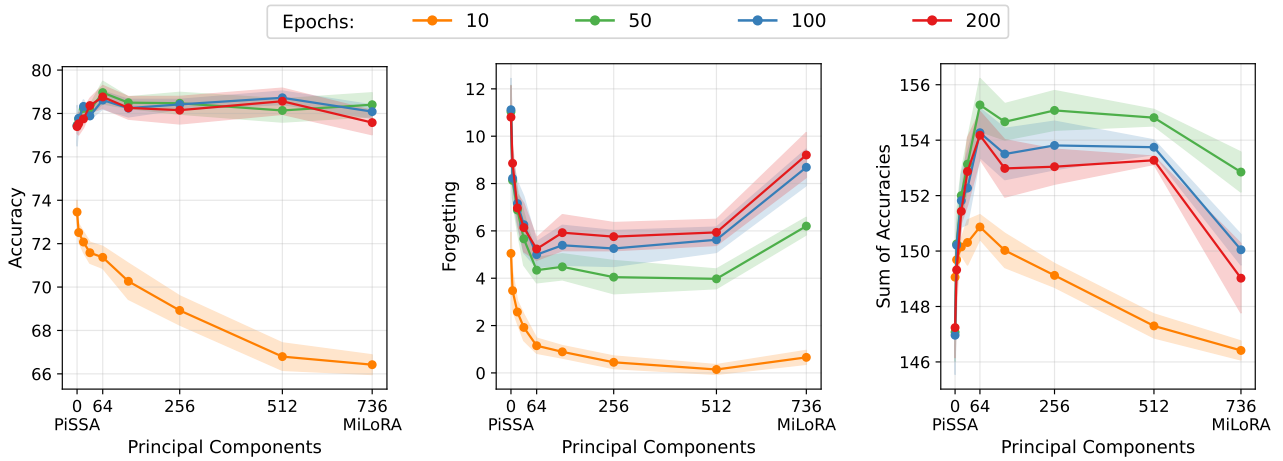


Figure 20. (ImageNet1k → DTD) Results of fine-tuning an ImageNet1k pre-trained ViT-Base to DTD using SPISSA with rank 32, using different starting points. From left to right, accuracy of DTD, forgetting of ImageNet1k, and sum of accuracies of DTD and ImageNet1k at the end of fine-tuning.

B.2. NLP

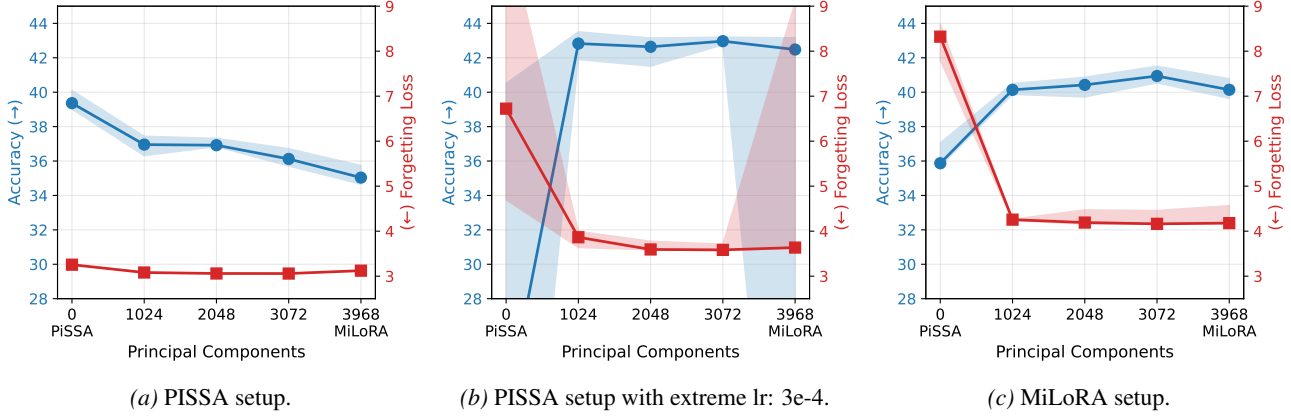


Figure 21. Mathematical reasoning results with LLaMA-2 7b. We report median and min/max. Outlier values correspond to runs with exploding gradients.

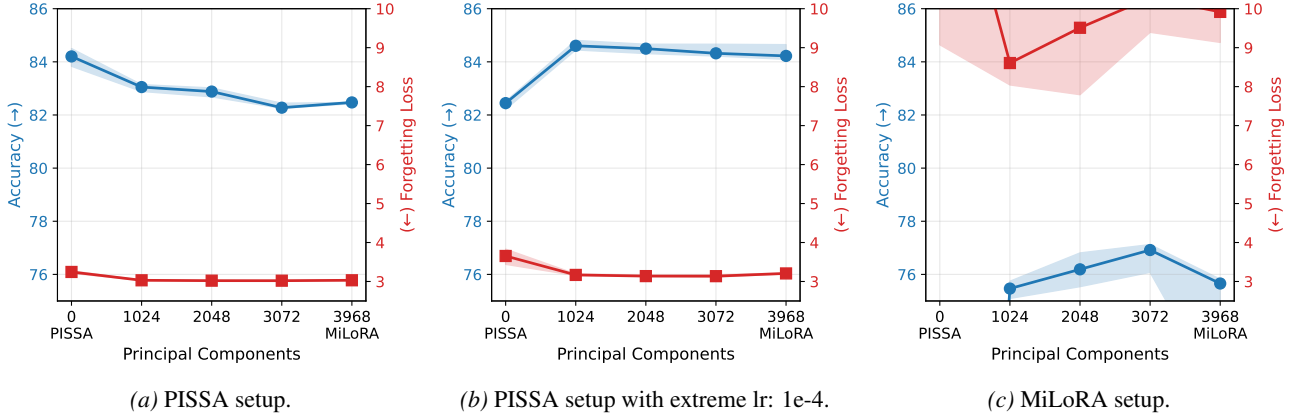


Figure 22. Common sense results with LLaMA-2 7b. We report median and min/max.

Table S2. Mathematical reasoning results with LLaMA-2 7b. We report mean and standard deviation over 4 independent runs. High standard deviations include runs with exploding gradients. We highlight **best** and second best.

Methods	MATH	GSM8K	Average (\uparrow)	Forgetting (\downarrow)
PiSSA	14.33 ± 0.30	64.59 ± 0.73	39.46 ± 0.50	3.26 ± 0.00
PiSSA (ours)	9.79 ± 9.82	32.75 ± 34.50	21.27 ± 22.16	7.23 ± 3.03
Ours (1024)	19.59 ± 0.14	65.94 ± 1.24	42.77 ± 0.67	3.84 ± 0.16
Ours (2048)	18.82 ± 0.39	66.15 ± 1.03	42.49 ± 0.69	3.64 ± 0.09
Ours (3072)	19.43 ± 0.16	66.51 ± 0.44	42.97 ± 0.25	3.61 ± 0.07
MiLoRA (ours)	14.02 ± 9.36	50.04 ± 33.36	32.03 ± 21.36	5.00 ± 2.73
MiLoRA	17.35 ± 0.62	63.00 ± 0.48	40.18 ± 0.47	4.27 ± 0.20

Table S3. Common sense results with LLaMA-2 7b. We report mean and standard deviation over 4 independent runs. We highlight **best** and second best.

Methods	BoolQ	PIQA	SIQA	HellaSwag	WinoGrande	ARC-e
PiSSA	74.62 ± 0.55	86.00 ± 0.46	81.53 ± 0.54	94.57 ± 0.26	86.78 ± 0.28	88.86 ± 0.49
PiSSA (ours)	73.06 ± 0.52	84.33 ± 0.63	80.62 ± 0.49	92.67 ± 0.28	84.87 ± 0.78	86.09 ± 0.92
Ours (1024)	75.04 ± 0.40	86.24 ± 0.69	81.36 ± 0.40	95.06 ± 0.06	86.90 ± 0.39	89.19 ± 0.57
Ours (2048)	74.68 ± 0.62	85.89 ± 0.17	81.47 ± 0.19	94.97 ± 0.12	86.44 ± 0.24	88.88 ± 0.58
Ours (3072)	74.54 ± 0.14	86.15 ± 0.40	81.13 ± 0.44	94.97 ± 0.17	87.10 ± 0.59	88.82 ± 0.29
MiLoRA (ours)	74.27 ± 0.52	86.10 ± 0.46	81.61 ± 0.14	94.91 ± 0.33	87.25 ± 0.56	89.07 ± 0.33
MiLoRA	69.72 ± 1.33	77.77 ± 1.96	75.67 ± 1.20	83.50 ± 4.01	77.05 ± 1.92	76.76 ± 2.75

Methods	ARC-c	OBQA	Average (\uparrow)	Forgetting (\downarrow)
PiSSA	75.83 ± 0.75	85.28 ± 1.16	84.19 ± 0.27	3.24 ± 0.04
PiSSA (ours)	73.02 ± 0.34	84.60 ± 1.14	82.41 ± 0.13	3.64 ± 0.20
Ours (1024)	76.09 ± 0.43	87.05 ± 0.41	84.62 ± 0.17	3.17 ± 0.02
Ours (2048)	77.05 ± 0.68	86.55 ± 0.77	84.49 ± 0.19	3.14 ± 0.01
Ours (3072)	76.54 ± 0.21	85.80 ± 1.10	84.38 ± 0.20	3.14 ± 0.03
MiLoRA (ours)	75.96 ± 0.34	85.20 ± 0.71	84.30 ± 0.25	3.21 ± 0.01
MiLoRA	61.35 ± 2.70	75.20 ± 2.47	74.63 ± 2.17	10.68 ± 2.14